Why High-Frequency Pulse Tubes Can Be Tipped

G. W. Swift and S. Backhaus

Condensed Matter and Magnet Science Group
Los Alamos National Laboratory
Los Alamos NM 87545

ABSTRACT

The typical low-frequency pulse-tube refrigerator loses significant cooling power when it is tipped with the pulse tube's cold end above its hot end, because natural convection in the pulse tube loads the cold heat exchanger. Yet most high-frequency pulse-tube refrigerators work well in any orientation with respect to gravity. In such a refrigerator, natural convection is suppressed by sufficiently fast velocity oscillations, via a nonlinear hydrodynamic effect that tends to align the density gradients in the pulse tube parallel to the oscillation direction.

Since gravity's tendency to cause convection is only linear in the pulse tube's end-to-end temperature difference while the oscillation's tendency to align density gradients with oscillating velocity should be quadratic in that temperature difference, it is easiest to suppress convection when the end-to-end temperature difference is largest. Simple experiments demonstrate this temperature dependence, the strong dependence on the oscillating velocity, and little or no dependence on the magnitude or phase of the oscillating pressure. In some circumstances in this apparatus, the suppression of convection is a hysteretic function of oscillating velocity. In some other circumstances, a time-dependent convective state seems more difficult to suppress.

INTRODUCTION

In the pulse tube of a pulse-tube refrigerator, acoustic power should be transmitted from cold to hot with as little dissipation as possible, while all processes that could carry heat from hot to cold should be minimized. A slender aspect ratio, careful flow straightening at the ends of the tube, and use of a low-conductivity material for the tube wall are among the design choices commonly made to minimize such heat flow.

Vertical operation, with the cold end of the pulse tube down, is among those common design choices for low-frequency pulse-tube refrigerators, because it makes the gas in the pulse tube stable against natural convection. However, it is often reported that high-frequency pulse-tube refrigerators work well in any orientation.[1-3] In this paper and an earlier, longer paper,[4] we describe and demonstrate the hydrodynamic mechanism responsible for suppressing natural convection in high-frequency pulse tubes. Figure 1 illustrates the physics.

Figure 1(a) shows the pulse tube of a pulse-tube refrigerator, oriented at a tip angle θ that puts its hot end below its cold end. Flow straighteners at both ends ensure that the oscillating displacement $a\cos\omega t$ is as uniform as possible across each cross section of the tube, while the

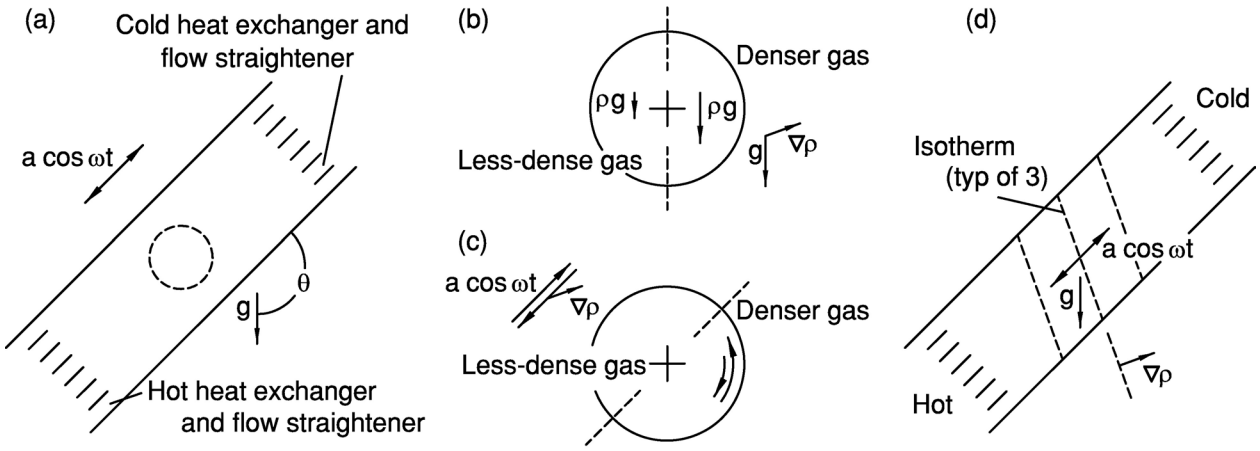

Figure 1. (a) A tipped pulse tube. The dashed circle shows a region of interest, which is carried along with the axial displacement $a \cos \omega t$. (b) The region of interest in (a) might be considered as a solid disk with temperature and density gradients. Gravity pulls more forcefully on the dense half of the disk, trying to align the density gradient with gravity, tending to turn the disk clockwise here. (c) If the density gradient is not parallel with the axial oscillation, the axial oscillation causes an angular oscillation. A nonlinear interaction between the axial and angular oscillations, as described in the text, then causes a net angular displacement every cycle, counterclockwise in this illustration. (d) A steady state can exist with the effects illustrated in (b) and (c) in balance and the density gradient pointing between the oscillation axis and gravity. Faster oscillations bring the density gradient closer to the oscillation axis, thus bringing the isotherms more nearly perpendicular to the oscillation axis.

displacement amplitude a generally depends on axial position because of the oscillating pressure and the gas's compressibility (and, in fact, the time phase of the displacement oscillation varies axially for the same reasons). Gravity g, pulling downwards, tends to cause the dense, cold gas near the cold heat exchanger to fall along the right/bottom wall and the less-dense, hot gas near the hot heat exchanger to rise along the top/left wall.

Although the overall motion of the gas in the pulse tube is complicated, to appreciate the physics of the convection-suppression mechanism we consider only a small disk-shaped region in the center of the pulse tube, shown by the dashed circle in Fig. 1(a), which we imagine behaving as a solid body that oscillates axially as $a \cos \omega t$ and may also rotate.

Figure 1(b) illustrates the response of this disk-shaped region to gravity. The density ρ of the gas is, on average, higher to the right of the vertical dashed line than to the left, because the cold heat exchanger is above and to the right of the hot heat exchanger. Appropriately averaging the density over the right and left halves of the disk, there is a greater force ρg pulling down on the right half of the disk than on the left half. The net torque tends to make the disk rotate clockwise; in the absence of any other effect, this would eventually align the disk's density gradient with gravity.

Figure 1(c) illustrates the simultaneous response of the disk to the axial oscillations $a \cos \omega t$. First, consider the half of the cycle during which the disk is moved up and to the right a distance $2a$. If the density were symmetrically distributed on both sides of the dashed line aligned with the oscillation direction, then this displacement would give the disk no tendency to rotate. However, the density is, in fact, higher to the right and below the dashed line than above and to its left, because natural convection has pulled dense gas down along the right and has floated less-dense gas up along the left. Thus, as the disk is displaced up and right by the motion, the extra inertia below the line causes the disk to rotate clockwise. Similarly, as it is displaced down and left it rotates counterclockwise.

The clockwise and counterclockwise rotations illustrated in Fig. 1(c) are not equal. For a rigid disk, the mathematics is straightforward[5] but the underlying physics[6] is subtle: The torque exerted on the disk during oscillation depends on the moment arm of the center of mass of the disk relative to the vibration axis, which in turn depends on the angular position of the disk (e.g.,

most obviously approaching zero as the density gradient aligns with the oscillation axis). The sign of this dependence of torque on angle causes a net counterclockwise angular change during each cycle for the circumstances of the illustration.

The time-averaged torque tending to align the disk's density gradient with the oscillation is proportional to the product of the amplitude of the angular oscillation and how strongly the torque caused by the oscillation varies with angle. Since both of these factors involve the density gradient, the tendency to align the density gradient with the oscillation axis is nonlinear in the end-to-end temperature difference.

Finally, Fig. 1(d) shows a balance between the clockwise tendency of Fig. 1(b) and the counterclockwise tendency of Fig. 1(c). A fast enough axial oscillation can hold the density gradient almost parallel with the oscillation direction, and thus hold the isotherms nearly perpendicular to the axis of the pulse tube, overcoming gravity's tendency to cause convection.

Reference 4 analyzes this balance under the simplifying assumption that any convective motion in the pulse tube can be treated as a single degree of freedom, showing at Eq. (29) that the suppression of convection should occur when the dimensionless pulse-tube-convection number

$$N_{ptc} = \frac{\omega^2 a^2}{g\,(\alpha D \sin\theta - L\cos\theta)} \left(\frac{\Delta T}{T_{\text{avg}}}\right)^{\beta} \gtrsim 2, \qquad (1)$$

where ω is the radian frequency of the oscillation and a is its displacement amplitude, so ωa is the velocity amplitude; g is the acceleration of gravity; D is the pulse-tube diameter and L is its length, ΔT is the end-to-end temperature difference, and T_{avg} is the average absolute temperature. The tip angle θ is taken to be zero in the vertical, gravitationally stable orientation, so both terms in the denominator are positive for the interesting range $90° \le \theta \le 180°$. The parameter α is a fitting parameter, experimentally found to be about 1.5, and experiment shows that β is close to 1/2 while the theory in Ref. 4 predicts $\beta = 1$. In Ref. 4, we calculated N_{ptc} using a in the middle of the pulse tube, but now we believe it is more useful to use a at whichever end of the pulse tube it is larger, for reasons explained below.

That high-frequency oscillations can suppress natural convection in fluids is well known to the large number of researchers whose work is summarized in Ref. 7, which establishes a foundation for analyzing such phenomena in three-dimensional, vector-calculus detail.

EXPERIMENTS

To investigate pulse-tube convection and its suppression by oscillating velocity under a broad range of experimental conditions, a tippable apparatus with interchangeable tubes much simpler than complete pulse-tube refrigerators was built. Three such tubes are shown in Fig. 2, and four more are shown in Ref. 4 together with a more complete description of other components. The pulse tubes were thin-walled stainless steel, bounded on each end by diffusion-bonded stainless-steel-screen flow straighteners and drilled copper heat exchangers. A linear motor and piston to the left of the parts shown in Fig. 2 created the oscillations at desired frequencies and amplitudes. Working only at and above ambient temperature allowed the use of easily measured electric-resistance heat, so "cold" was near room temperature and "hot" was considerably higher in these measurements.

Raw data and hysteresis

Figure 3(a) shows a typical raw data set obtained with the setup of Fig. 2(c). The vertical axis shows Q, the heater power required to maintain the hot-heat-exchanger thermocouple at 250°C, and the horizontal axis shows the ratio of pressure amplitude p_a in the bounce space to mean pressure p_m.

With this tube oriented at zero degrees, i.e., with the cold end down, the lower data set in Fig. 3(a) shows the measured heat rising with oscillation amplitude from 21 to 23 W. Simple

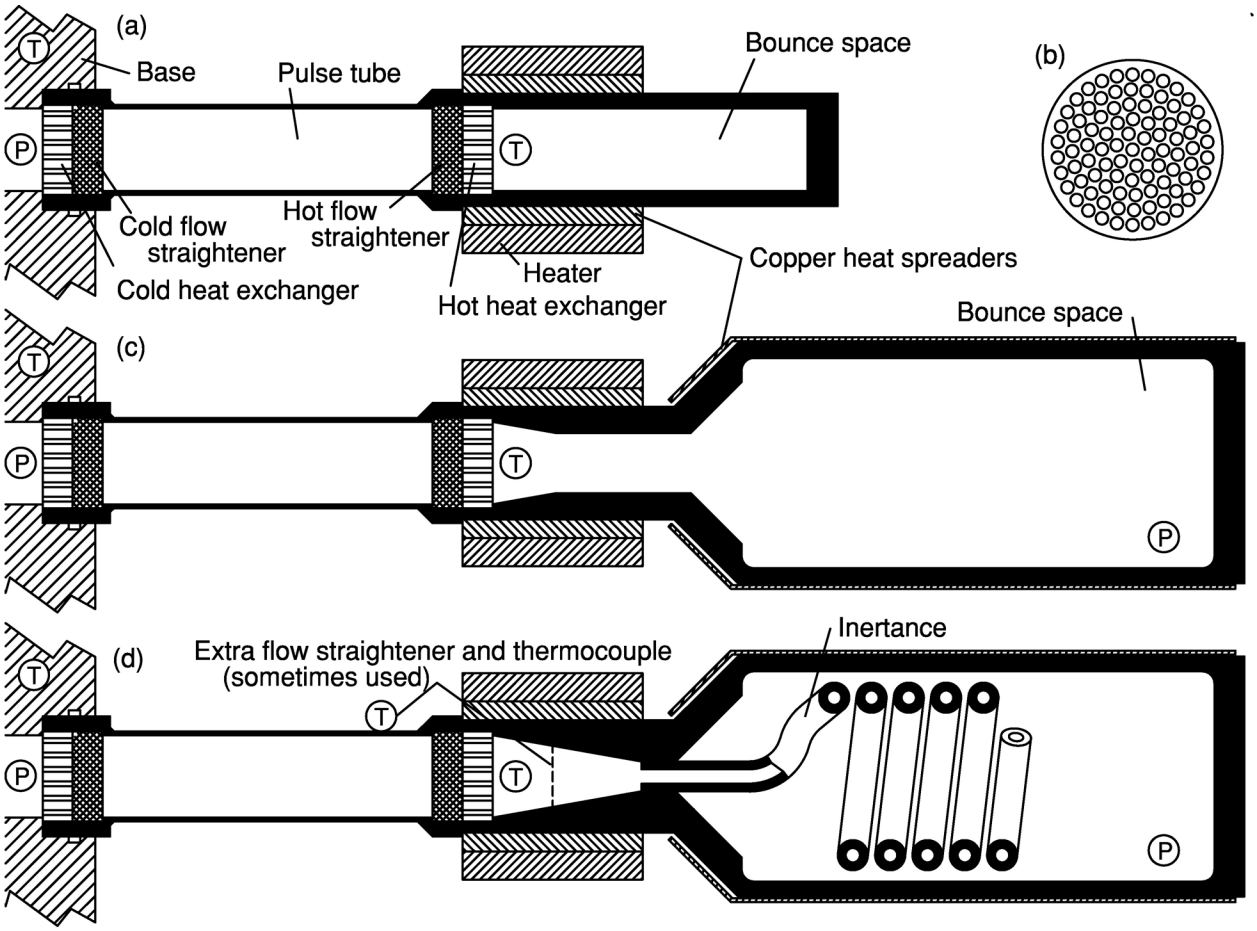

Figure 2. Three setups for measurements with a pulse tube of length 6.99 cm and diameter 1.74 cm. P and T denote pressure transducers and thermocouples, respectively. (a) In this setup, one of five tubes described in detail in Ref. 4, the time phasing between pressure and velocity is nearly that of a standing wave, and the bounce space is small enough that the displacement a varies strongly from one end of the pulse tube to the other. (b) The hole pattern in each heat exchanger, at twice the scale of (a). (c) The same pulse tube as in (a), but with a much larger bounce space to reduce the end-to-end variation of a in the pulse tube. (d) The same pulse tube as in (a) and (b), but with a long, coiled inertance tube between the pulse tube and the bounce space, to change the time phasing between oscillating velocity and oscillating pressure in the pulse tube.

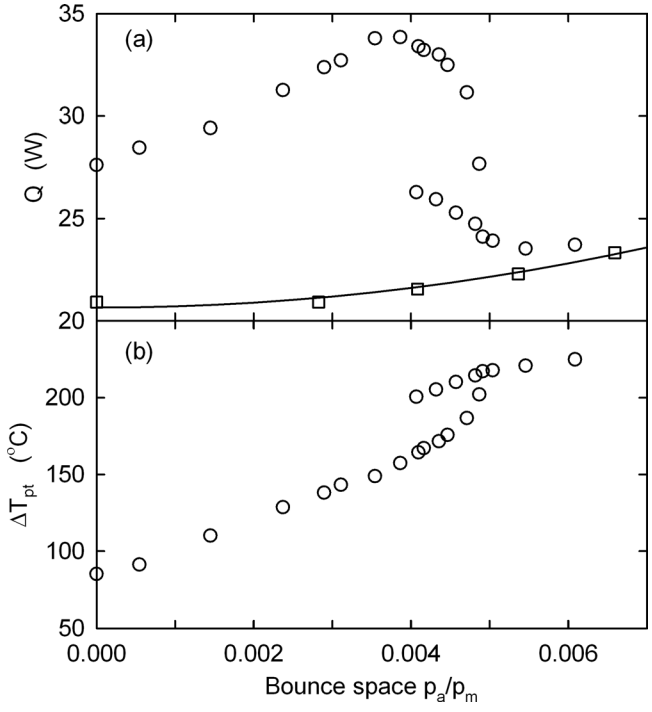

Figure 3. (a) Heat Q required to maintain the hot thermocouple at 250°C while the base was held at 10 to 12°C in the tube of Fig. 2(c), with helium gas at a mean pressure p_m = 3.1 MPa and a frequency of 100 Hz. Squares, tube oriented vertically; the curve (Q_{vert}) is a quadratic fit to the squares. Circles, tube tipped at θ = 120° from vertical; the upper and lower branches show hysteresis in the transition. (b) Calculated temperature difference across the column of gas in the pulse tube, for the same circumstances.

calculations show that the thermal conductivity of the gas and the metal of the pulse tube itself contribute only 0.15 W and 2.5 W, respectively, so most of the 21 W needed at zero amplitude is heat leak from the hot parts to the room through ceramic-fiber insulation not shown in Fig. 2. For subsequent data analysis, we subtracted a smooth curve that fit this baseline, Q_{vert}, from measurements with the tube tipped, to obtain the extra heat due to tipping.

Figure 3(a) shows that an additional 6 W is carried by convection at zero amplitude with the tube oriented at 120°. At first, this additional heat rises significantly with amplitude. When Ref. 4 was written, this initial increase of Q with amplitude was unexplained, but now we believe that it is simply due to the temperature drops across the flow straighteners. The convective heat must flow axially through the flow straighteners (and the surrounding tube wall, in parallel), so the temperature difference across the convecting gas itself is significantly smaller than the temperature difference measured by the thermocouples in this apparatus. As the amplitude rises, the temperature difference across the flow straighteners is reduced by rapidly moving gas and imperfect thermal contact in the flow straighteners (which are much coarser than a regenerator would be under these circumstances), so the temperature difference applied across the convecting gas rises; consequently, the convective heat flow rises, too. We used DELTAEC [8] STKSCREEN segments to model the flow straighteners under these conditions, forcing $Q–Q_{vert}$ extra heat through the STKSCREEN segments to obtain an estimate ΔT_{pt} of the temperature difference across the convection cell inside the pulse tube. For the effective conductance of stacked stainless-steel screens, Ref. 9 recommends using a fraction $f_c = 0.1$ of the conductance of a geometrically idealized structure of equal porosity, but to that we must add something for the surrounding tube wall. Although the full tube-wall thickness would yield a total $f_c = 3$, the lateral thermal contact between the tube wall and the flow-straightener–convection-cell interface is imperfect, so the most realistic value must be less than 3. For Fig. 3, we found that using f_c in the range of 1.0 to 1.2 yielded a convective Nusselt number independent of, or rising weakly with, ΔT_{pt}. We adopted $f_c = 1.0$ for subsequent analysis. For the data of Fig. 3(a), this process yields the estimate for ΔT_{pt} shown in Fig. 3(b).

In the range $0.004 < p_a/p_m < 0.005$, Fig. 3(a) shows that the extra heat $Q–Q_{vert}$ needed to maintain the hot thermocouple near 250°C dropped abruptly, and hysteretically, to near zero, as the oscillations suppressed the convection according to the process described in the Introduction. At least some of the hysteresis may be due to the significant temperature drops across the flow straighteners described in the previous paragraph. In the hysteretic region, it is possible for the convection to be suppressed, the heat flowing through the flow straighteners to be reduced, the end-to-end temperature difference across the pulse tube to be relatively large, and hence the velocity needed to suppress convection to be relatively low; and it is also possible for the convection to be active, the heat flow through the flow straighteners to be large, the end-to-end temperature difference across the pulse tube to be somewhat reduced, and hence the velocity needed to suppress convection to be somewhat increased. Thus, at least some of the observed hysteresis is probably due to a combination of the unfortunately large flow-straightener temperature drops in this hardware and the counter-intuitive fact that the convection-suppression process rises more rapidly with ΔT_{pt} than does gravity-driven convection itself.

Dependence on temperature, frequency, and amplitude

Reference 4 shows experimental evidence that the transition between natural convection and the oscillation-induced suppression of convection occurs near $N_{ptc} = 1$ for a wide range of conditions for most of the tubes studied, where N_{ptc} was calculated based on the velocity amplitude in the *middle* of the pulse tube and on the difference ΔT between the thermocouple temperatures. Re-analyzing those measurements using ΔT_{pt} (instead of the difference between the thermocouple temperatures) in Eq. (1) shifts the transition down about 30% but does not change any of Ref. 4's conclusions about the form of Eq. (1) or the values of α and β. For example, Fig. 4 shows measurements at three different hot temperatures, and hence three different ranges of ΔT_{pt}, which were shown in Fig. 5(b) in Ref. 4 but are re-analyzed here with

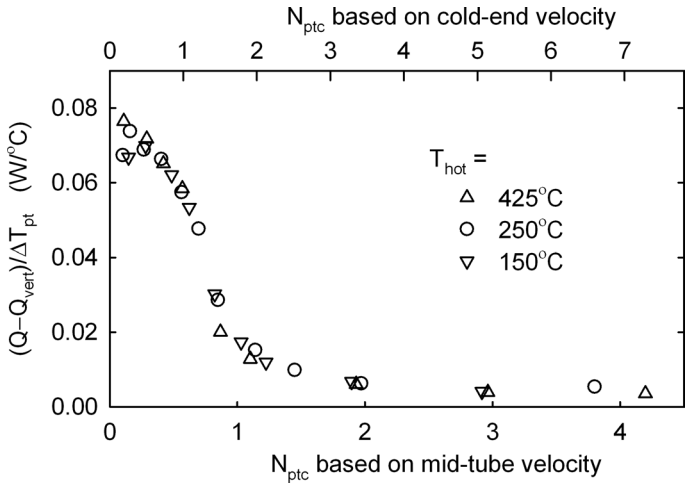

Figure 4. Convection conductance vs N_{ptc} for three different hot temperatures, all with $T_{cold} \sim 20^{o}C$, in 3.1-MPa helium at 100 Hz in the setup of Fig. 2(a). These are the same data shown in Ref. 4, Fig. 5(b), but here using ΔT_{pt} instead of the thermocouple temperature difference in the horizontal axis. This graph uses $\beta = ½$ in N_{ptc}. As shown in Ref. 4, using $\beta = 1$ ruins the agreement among the three data sets.

ΔT_{pt} used in Eq. (1). That these three sets of data fall on a common curve in Fig. 4 supports the use of $\beta = 1/2$ in Eq. (1).

In this section, we show additional evidence that N_{ptc} governs the convection-suppression transition, continuing to use ΔT_{pt} for the analysis of the data.

The circles in Fig. 5(a) show the 100-Hz data of Fig. 3 expressed in terms of N_{ptc}. For each data point, a DELTAEC model[8] was matched to the experimental values of p_m, p_a, ω, the thermocouple temperatures, and the convective heat flow, and the results of each model included ΔT_{pt} and the gas displacement amplitude a throughout the pulse tube. A set of data with the same apparatus but with a frequency of only 45 Hz is also shown in Fig. 5(a). The good alignment of these two data sets, despite more than a factor of two difference in frequency (which appears squared in N_{ptc}), is good confirmation that the product ωa, i.e., the velocity amplitude, captures the important frequency and amplitude dependence of the transition.

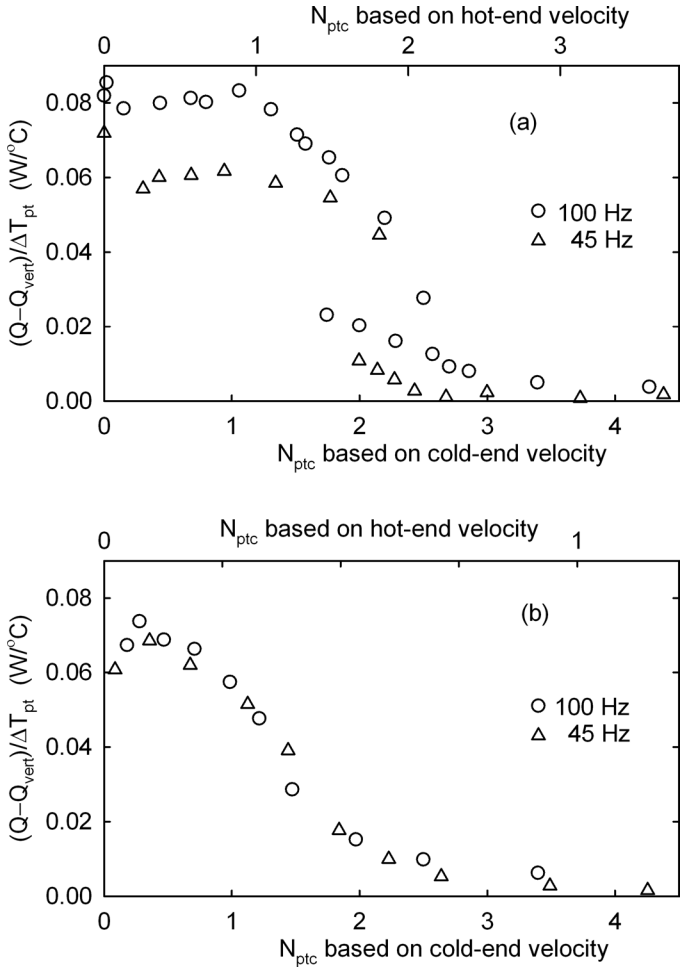

Figure 5. Convection conductance vs pulse-tube-convection number at two frequencies in 3.1-MPa helium. On the bottom axes, N_{ptc} is calculated using the velocity at the cold end of the pulse tube, where the velocity is highest. Auxiliary (top) axes show how different that axis would be if the hot end were used. (a) Measurements with the setup of Fig. 2(c), i.e., a relatively low p_a/p_m and low end-to-end velocity variation. The 100-Hz data are also shown in Fig. 3. (b) Measurements with the setup of Fig. 2(a), i.e., with a higher p_a/p_m and higher end-to-end velocity variation. (These data also appear in Ref. 4, Fig. 4(b), where the mid-tube velocity was used.)

Figure 5(b) shows two comparable data sets from Ref. 4. That previous work used ωa at the middle of the pulse tube for calculation of N_{ptc} (and used the thermocouple temperature difference), but here we show horizontal axes using ωa at both ends, and using ΔT_{pt} instead of the thermocouple temperature difference. We lined up parts (a) and (b) of Fig. 5 with equal scaling on N_{ptc} using cold-end velocities, because we now realize that the transition to suppressed convection should begin at the high-velocity end of the tube: The Nusselt number for convection in this cell is approximately 40, so the conductance of the cell should be reduced dramatically by even a relatively short region of suppressed convection near the high-velocity end. In Figs. 4 and 5, the suppression of convection occurs near $N_{ptc} \sim 2$ at the cold end.

Time-dependent convection

To explore another set of circumstances, we used the apparatus shown in Fig. 2(d), which included an inertance tube between the pulse tube and the bounce space, to allow unequal pressure amplitudes in those two spaces, and thus allow a wider variety of relative amplitudes and time phasing between oscillating motion and oscillating pressure. To obtain the velocity ωa

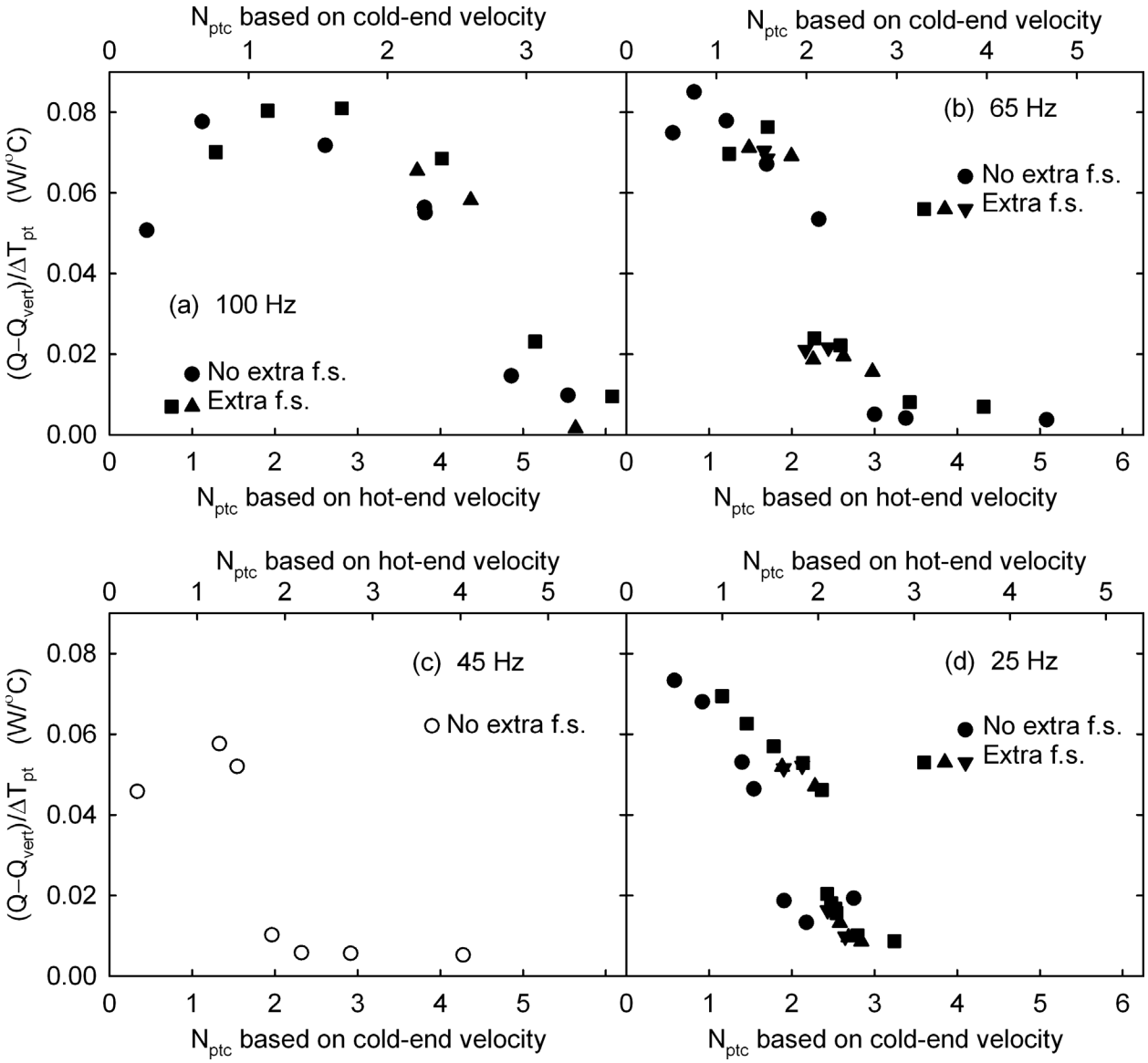

Figure 6. Convection conductance vs pulse-tube convection number, at four different frequencies, in the tube of Fig. 2(d) with 3.1-MPa helium gas and $T_{hot} = 250\,^{o}C$. The primary horizontal axes, which all run from 0 to 6.25, use the fastest velocity in the tube, and the upper horizontal axes use the slowest velocity. Unfilled symbols are used for the lone case of steady convection in this figure, and filled symbols denote time-dependent convection.

from each measurement, we forced a DELTAEC model to match the measured temperatures and pressure phasors, using the inertance-tube's cross-sectional area and perimeter as fitting parameters so both of the pressure phasors could be matched. This process usually required that the fitting area be 85–95% of the inside area of the inertance tube before it was coiled and that the fitting perimeter be 100–120% of the inside perimeter before coiling. This area range seems reasonable, since coiling a tube decreases its cross-sectional area; and the perimeter range, and its dependences on amplitude and frequency, are roughly compatible with the known increase in dissipation in oscillating flow when a tube is coiled.[10] Results of each DELTAEC model included, as before, the temperatures and velocities at the ends of the pulse tube, which were used to express the experimental results in terms of $(Q-Q_{vert})/\Delta T_{pt}$ vs N_{ptc}, as shown in Fig. 6. (The velocities obtained in this way are essentially identical to those that result straightforwardly from treating the bounce space and pulse tube as adiabatic cavities subject to the measured pressure phasors, with the intervening inertance tube, hot heat exchanger, and hot flow straightener as having negligible volumes, but we found it easier to obtain the velocities via DELTAEC since we also needed ΔT_{pt}.)

The temperature in the gas near the hot heat exchanger was sensed with a 1.6-mm-diam, sheathed, type-K thermocouple, which was connected to a digital readout with 0.1°C resolution and to a paper strip-chart recorder with slightly lower resolution. Sometimes during these measurements and those of Ref. 4, that temperature seemed steady in time, to the limits of the instrumental resolution, but at other times a small time dependence was visible in the hot temperature, with erratic changes of up to a few tenths of a degree occurring over time scales of many tens of seconds. Near the end of the present measurements, wondering whether this time dependence might be the result of time-dependent convection in the pulse tube, we added another thermocouple to the pulse-tube wall near the hot heat exchanger. When the hot thermocouple exhibited time-dependent temperature, this new thermocouple also showed time dependence, with a magnitude roughly five times higher. Thus, it seems likely that the convection in this pulse tube is sometimes time dependent. (See Ref. 11 for a recent review of the vast literature on time-dependent convection, without superimposed acoustic oscillations.) In all figures in this paper, steady-temperature measurements are indicated by open symbols, and measurements that exhibited time-dependent temperatures are indicated with filled symbols.

Early in this set of measurements, the "extra flow straightener" shown in Fig. 2(d) was not present. Wondering whether the high values of N_{ptc} obtained in the 100-Hz data set in Fig. 6(a) arose from imperfect flow straightening of the jet impinging on the hot heat exchanger from the adjacent end of the inertance, or whether the time dependence we sometimes observed was caused by such a jet, we added that extra flow straightener and repeated some of the measurements, which showed a significant change at one frequency, shown in Figs. 6(d), and smaller or no significant differences at two other frequencies, shown in Figs. 6(a) and (b). Additional, brief measurements were also made with another extra flow straightener between the cold heat exchanger and the piston, and with changes to the insulation around the hot parts. These changes made little or no difference.

As shown in Table 1, all of the measurements discussed here and in Ref. 4 are consistent with the hypothesis that steady convection experiences its convection-suppression transition at $N_{ptc} \sim 2$, where N_{ptc} is calculated with Eq. (1) using the velocity at the fast end of the tube, and that time-dependent convection requires higher N_{ptc}. In Ref. 4, measurements with $D/L = 0.13$ and 0.25 were steady while those with $D/L = 0.52$, 0.75, and 1.57 were time dependent, and the $D/L = 0.75$ and 1.57 tubes required higher N_{ptc} than the others. In Fig. 6 here, only the 45-Hz data set showed steady temperature, and it had the lowest transition N_{ptc}, comparable to the transition N_{ptc} in the steady-temperature data of Fig. 5. The time dependence may be an artifact of the poor thermal conductance of the flow straighteners in the present apparatus, or it may be inherent to these pulse-tube conditions.

It is also interesting to note that some of the 65-Hz and 25-Hz data exhibited hysteresis with respect to the applied pressure amplitudes, qualitatively similar to that shown in Fig. 3(a) but narrower. However, this hysteresis does not appear in Figs. 6(b) and 6(d) because of the strong

Table 1. Summary of parameters at the middle of the transition from convection to suppression, for 3.1-MPa helium and a tip angle of $\theta = 120^{\circ}$. Here N_{ptc} is based on fast-end velocity and ΔT_{pt}, so these values differ from those reported in Ref. 4. Angle φ is the phase by which pressure leads velocity at the middle of the pulse tube, and p_a/p_m is the ratio of pressure amplitude to mean pressure, which varies little from one end of the pulse tube to the other. The transition from steady convection occurs at $N_{ptc} \sim 1\frac{1}{2}$ to 2, over a broad range of p_a/p_m and φ, while suppression of time-dependent convection requires higher N_{ptc}.

Fig. number	*D/L*	Freq. (Hz)	Conv. type	N_{ptc}	p_a/p_m	φ (degrees)
4	0.25	100	steady	1½	0.020	–89
5(a)	0.25	100	steady	2	0.004	–90
5(a)	0.25	45	steady	2	0.010	–90
5(b)	0.25	100	steady	1½	0.021	–89
5(b)	0.25	45	steady	1½	0.046	–89
6(c)	0.25	45	steady	1¾	0.006	–37
7(c) in Ref. 4	0.13	100	steady	1	0.016	–89
7(c) in Ref. 4	0.25	100	steady	1½	0.020	–89
6(a)	0.25	100	time-dep.	4–4½	0.023	+41
6(b)	0.25	65	time-dep.	2–2½	0.008	+21
6(d)	0.25	25	time-dep.	1½–2½	0.016	–71
7(c) in Ref. 4	0.52	100	time-dep.	1½	0.025	–90
7(c) in Ref. 4	0.75	100	time-dep.	3½	0.025	–90
7(d) in Ref. 4	1.57	100	time-dep.	3½	0.029	–90

dependence of the estimated temperature drops across the flow straighteners on whether or not the gas is convecting and the consequences for calculating N_{ptc} via ΔT_{pt}. Thus, in these cases, it appears that the flow-straightener temperature drops were responsible for *all* of the observed hysteresis.

CONCLUSIONS

The rapid oscillating velocity ωa in the pulse tube of a high-frequency pulse-tube refrigerator can stop natural convection via an interesting hydrodynamic process that tends to align density gradients with the oscillation direction. Oscillating pressure seems to be of only indirect importance, by causing spatial nonuniformity in the velocity via the gas compressibility.

The convection-suppression transition can be hysteretic if the end-to-end velocity difference is small enough and the convective state is steady or nearly so. However, some of the hysteresis may be an artifact of the poor thermal conductance of the flow straighteners used in these measurements.

Based on the evidence here and in Ref. 4, steady convection is suppressed when $N_{ptc} > 2$ in tubes with small aspect ratios *D/L*, where N_{ptc} is given by Eq. (1) and is calculated based on the end temperatures of the column of gas in the pulse tube and on the velocity ωa at whichever end of the pulse tube is fastest. Other tubes in Ref. 4 that had bigger aspect ratios, and some cases in the present measurements, exhibited time-dependent convection, which seems harder to suppress, requiring N_{ptc} to be roughly two times larger.

Future, similar experimental work investigating the fundamentals of this phenomenon should use copper instead of stainless steel for flow straighteners, to provide more nearly isothermal boundary conditions on the ends of the tube and to tie the gas temperatures more closely to the heat-exchanger temperatures. If an inertance tube is used, then tighter flow straighteners (or flow straighteners on both sides of the heat exchanger) should also be considered, to insure against a jet from the inertance tube disturbing the pulse tube, in case this is the source of some of the observed time dependence. Thermometers better attached to the heat

exchangers or flow straighteners, and perhaps additional thermometers on the pulse-tube side walls, would also help clarify understanding, especially of the time-dependent convective states. (Alternatively, a gas-filled cylinder with closed ends could be shaken axially, completely eliminating the need for porous heat exchangers and flow straighteners for such measurements, though also eliminating the end-to-end variation in ωa that is essential to the operation of real pulse tube refrigerators.)

Future theoretical and computational studies could be based on the general foundation reviewed in Ref. 7.

ACKNOWLEDGMENT

This work was supported by license income from thermoacoustic patents at Los Alamos National Laboratory.

REFERENCES

1. Thummes, G., Schreiber, M., Landgraf, R., and Heiden, C., "Convective Heat Losses in Pulse Tube Cryocoolers: Effect of Pulse Tube Inclination," *Cryocoolers 9,* Plenum, New York (1997), pp. 393-402.
2. Thummes, G., and Yang, L., "Development of Stirling-Type Pulse Tube Coolers Driven by Commercial Linear Compressors," *Infrared Technology and Applications XXVIII,* Society of Phot-Optical Instrumentation Engineering, Seattle (2003), pp. 1-14.
3. Wang, C., and Gifford, P.E., "A Single-Stage Pulse Tube Cryocooler for Horizontally Cooling HTS MRI Probe," *Advances in Cryogenic Engineering,* vol. 49, American Institute of Physics, New York (2004), pp. 1805-1811.
4. Swift, G.W., and Backhaus, S., "The Pulse Tube and the Pendulum," *Journal of the Acoustical Society of America,* vol. 126, no. 5 (2009), pp. 2273-2284.
5. Blitzer, L., "Inverted Pendulum," *American Journal of Physics,* vol. 33 (1965), pp. 1076-1078.
6. Butikov, E.I., "On the Dynamic Stabilization of an Inverted Pendulum," *American Journal of Physics,* vol. 69 (2001), pp. 755-768.
7. Gershuni, G.Z., and Lyubimov, D.V., *Thermal Vibration Convection*, Wiley, New York (1998).
8. Ward, W.C., Clark, J., and Swift, G.W., Design Environment for Low-Amplitude Thermoacoustic Energy Conversion (DELTAEC), software and user's guide freely available from the Los Alamos thermoacoustics web site www.lanl.gov/thermoacoustics/ . A typical model used for the analysis of the data in the present paper can be found at www.lanl.gov/thermoacoustics/Pubs near the preprint for this ICC-16 paper.
9. Lewis, M.A., Kuriyama, T., Kuriyama, F., and Radebaugh, R., "Measurement of Heat Conduction through Stacked Screens," Advances in Cryogenic Engineering, vol. 43, Springer, New York (1998), pp. 1611-1618. Note that f_c in this paper is called ksFrac in Ref. 8.
10. Olson, J.R., and Swift, G.W., "Energy Dissipation in Oscillating Flow through Straight and Coiled Pipes," *Journal of the Acoustical Society of America*, vol. 100, no. 4 (1996) pp. 2123-2131.
11. Ahlers, G., Grossman, S., and Lohse, D., "Heat Transfer and Large Scale Dynamics in Turbulent Rayleigh-Bénard Convection," *Reviews of Modern Physics*, vol. 81 (2009), pp. 503-537.